Structural and magnetic properties of undoped and Mn doped CdS nanoparticles prepared by chemical co-precipitation method

Nikita H. Patel[*], M.P. Deshpande, Sandip V. Bhatt, Kamakshi R. Patel, S. H. Chaki

Department of Physics, Sardar Patel University, Vallabh Vidyanagar 388120, Gujarat, India

[*]Corresponding author. Tel: (+91) 269 2226844; E-mail: nhptl123@yahoo.com

ABSTRACT

Undoped and Mn doped CdS nanoparticles with varying Mn concentration of 10,15 and 20 mol % have been prepared by chemical co-precipitation method with polyvinylpyrrolidone (PVP) as capping agent at room temperature. EDAX has shown that no foreign impurities are present in the synthesized nanoparticles and X-ray diffraction (XRD) revealed that undoped and Mn doped CdS nanoparticles possess cubic phase with crystallite size ranging from 4-6 nm. Transmission electron microscopy (TEM) images indicated that nanoparticle sizes are between 2-6 nm and exhibits polycrystalline nature as seen from selected area electron diffraction (SAED) pattern. Raman spectra of undoped and Mn-doped CdS nanoparticles have shown 1LO and 2LO phonon modes and their intensity ratio decreases as Mn concentration increases. Magnetic susceptibility clearly pointed out that undoped CdS behaves as diamagnetic whereas Mn doped CdS as paramagnetic and varies nonlinearly with Mn concentration in CdS. Rapid increase in magnetization below 50 K temperature is observed in M-T curves which can be assigned to Mn ions isolated in CdS crystal field or extrinsic defects. The M-H curve at 5 K and 300 K for 20% Mn doped CdS nanoparticles at different magnetic fields showed no hystersis. In near future Mn doped CdS nanoparticles can be used for application in dilute magnetic semiconductor and fabrication of solar cells. The result and discussion drawn from this work are elaborated in detail in the paper. Copyright © 2014 VBRI press.

Keywords: Mn doped CdS nanoparticles; XRD; Raman spectra; Gouy method; VSM.

Nikita H. Patel is doing Ph.D. from Department of Physics, Sardar Patel University, Vallabh Vidyanagar, Gujarat, India. Since 2011 in the field of synthesis and characterization of semiconductor nanomaterials.

M. P. Deshpande did his Ph.D. in the field of crystal growth and characterization in the year 1998 from Department of Physics, Sardar Patel University, Vallabh Vidyanagar, Gujarat, India. At present he is involved in the field of synthesis of metal and semiconductor nanomaterials by chemical route and their application in antimicrobial activity. Apart from this he is also doing the work in the field of Raman Spectroscopy of different layered semiconductors at high pressures using diamond anvil cell.

Introduction

In the past few years diluted magnetic semiconducting (DMS) nanoparticles have found their potential use in various fields like material science, high density recording media, spin valves, magnetic resonance imaging, ferro fluid technology, magneto caloric refrigeration and environmental areas. [1]. In DMS systems, magnetic ions randomly substitute the host semiconductor cations, and therefore are of potential use in electronic devices [2-4]. To integrate the DMS materials into electronic devices, it is important to have low-dimensional structures in order to gain advantages offered by the spins.

II–VI based semiconductors in nanoregime, cadmium sulfide (CdS) is one of the most important semiconductors having bulk band gap of 2.42 eV at room temperature [5] and exciton Bohr radius of 5.8 nm [6]. Among the nanocrystalline semiconductors, cadmium sulfide is investigated because of its importance in the field of nonlinear optics, light-emitting diodes, solar energy conversion, thin film transistors, gas detectors, optoelectronics, photo catalysis, photovoltaic cells, X-ray detectors and as a window material for hetero-junction solar cells due to its high absorption coefficient [7]. In low

dimensional semiconductors optical phonon modes behave substantially different from the bulk and optical phonons confined in semiconductor QDs affect the electronic properties responsible for Raman scattering. Most of the experimental studies of optical phonons in QDs have been performed by Raman spectroscopy [8]. Recently, spectroscopic studies of transition metal and rare-earth doped nanocrystalline CdS have motivated researchers to develop new and more efficient multicolor phosphor materials [9]. CdS based dilute magnetic semiconductor (DMS) materials have been extensively studied since they are highly multifunctional owing to their contemporaneous magnetic, semiconducting, electromechanical and optical properties [10, 11]. Undoped CdS layer results in poorer photovoltaic performance of the device [12]. Therefore, doping is the important step in preparation of CdS active elements for photovoltaics.

Investigation of CdS nanostructure has received increasing attention due to their size dependent properties and quantized charging effects in metal nanoparticles provide the basis for developing new and effective systems. These nanostructures provide innovative strategies for designing next generation energy conversion devices. Mn^{2+} has been the most extensively studied luminescence activator in II–VI semiconductor nanoparticles [13, 14]. Mn^{2+} doped CdS nanoparticles are interesting because of the fact that Mn^{2+} ions provide good traps for the excited electrons, which gives rise to their potential use in nonlinear optics, electronic and optoelectronic devices [14, 15]. These exciting achievements motivated us to investigate Mn^{2+} doped CdS nanoparticles. Mn-doped CdS materials have been synthesized in the form of nanocrystals inside a glass matrix and also as thin films [16]. There are several techniques to synthesize Mn^{2+} doped CdS nanoparticles such as. coprecipitation method, sonochemical method, sol–gel method and reverse micelles method, etc. [17].

The objectives of this work is to synthesize Mn doped CdS nanoparticles by chemical co-precipitation method with different molar percentage of Mn^{2+} ions at room temperature using polyvinylpyrrolidone (PVP), a water-soluble polymer, as a capping agent to stabilize the CdS nanoparticles. The structure of Mn doped CdS nanoparticles are studied by X-ray diffraction (XRD), transmission electron microscopy (TEM) and Raman spectroscopy. The magnetic properties are studied by Gouy method and vibrating sample magnetometer (VSM). The influence of dopant concentrations (Mn^{2+}) on the structural and magnetic properties of CdS nanoparticles is investigated and results are presented in the paper.

Experimental

Materials

The chemicals used for the preparation were analytical grade cadmium acetate dihydrate [$(CH_3COO)_2$ $Cd^.2H_2O$] (99%) purchased from Himedia Lab Pvt. Ltd., Mumbai. Manganese acetate tetrahydrate [$Mn(CH_3COO)_2^.4H_2O$] (98.5%, AR grade) purchased from Loba chemie also sodium sulphite monohydrate [$Na_2S^.H_2O$] (98%) and polyvinyl pyrolidone purchased from Chiti-Chem Corporation, Baroda.

Method

Undoped and Mn doped CdS nanoparticles were synthesized by chemical co-precipitation method at room temperature. Cadmium acetate dihydrate [$Cd(CH_3COO)_2^.2H_2O$], manganese acetate tetrahydrate [$Mn(CH_3COO)_2^.4H_2O$] and sodium sulphite monohydrate [$Na_2S^.H_2O$] were used as precursors and double distilled water as the solvent. 0.2M aqueous solution of cadmium acetate dihydrate and 5% (w/v) polyvinylpyrrolidone (PVP) were mixed together by stirring for 30 min. Then 0.2M aqueous solution of sodium sulphite monohydrate was added drop wise to the prepared solution (cadmium acetate+ PVP) and stirred for 15 min. The precipitate with yellowish color formed soon were filtered, washed number of times in distilled water and dried in a vacuum. However, in 10, 15, 20 mol % Mn doped CdS nanoparticles 0.2M aqueous solution of cadmium acetate and 0.02M, 0.03M 0.04M aqueous solution of manganese acetate were added at beginning for maintaining the nominal $[Cd^{+2}]:[Mn^{+2}]$ ratio respectively.
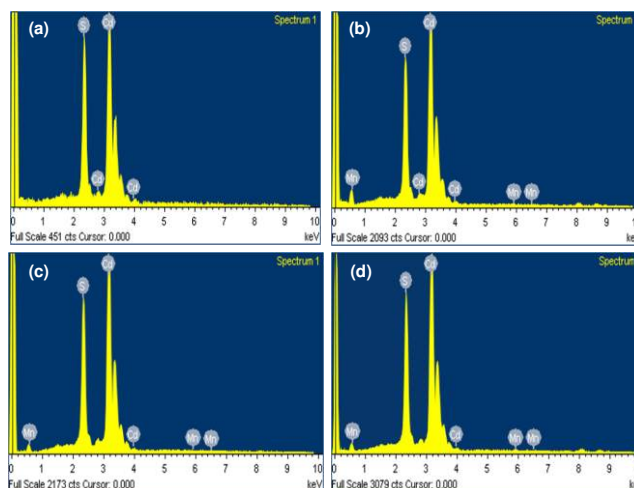

Fig. 1. EDAX spectra of undoped and Mn doped CdS nanoparticles.(a) CdS (b) 10 mol % Mn doped CdS (c) 15 mol % Mn doped CdS (d) 20 mol % Mn doped CdS.

Table 1. Wt% and At% of undoped and Mn doped CdS.

Sample	Wt%			At%		
	Cd	S	Mn	Cd	S	Mn
CdS	80.21	19.79	-	53.63	46.37	-
10% Mn doped CdS	80.25	19.63	0.12	53.75	46.09	0.17
15% Mn doped CdS	80.32	19.49	0.2	53.9	45.84	0.27
20% Mn doped CdS	79.89	19.61	0.5	53.38	45.93	0.69

The presence of the elements Cd, S, Mn was identified from the EDAX spectra obtained on model JOEL JSM-5610. Structural analysis were carried out using Philips Xpert MPD powder X-ray diffractometer with CuKα radiation (λ=1.54 Å). TEM images were taken to know the particle size and shape of the nanoparticles by using TEM with CCD camera Philips, Tecnai 20 at an operating voltage of 200 kV. Crystallographic information was also availed by bright field image selected area electron diffraction pattern from TEM. Raman spectra were obtained with excitation wavelength of 488nm Argon (Ar⁺)

laser as excitation source. Magnetic Susceptibility was determined using Gouy method whereas VSM measurements were carried out on 14T PPMS-Vibrating Sample Magnetometer in the temperature range 2 to 350 K and magnetic field upto 140 kOe with Sensitivity ~ 10-5 emu, temperature stability ~ 10 mK.

Results and discussion

Elemental study by energy dispersive analysis of X-rays (EDAX)

Fig. 1. (a, b, c, d) shows the EDAX spectra of undoped and Mn doped CdS nanoparticles which reveal that no other foreign impurities are present in the samples. **Table 1** provides the Wt% and At% obtained from these spectra indicating presence of better proportions of Cd: S: Mn in all the samples.

Structural properties

X-ray diffraction (XRD): The X-ray diffraction pattern shown in **Fig. 2** is analyzed by powder X software for undoped and Mn doped CdS samples. They all matched with the cubic zincblende structure without any impurity phase indicating a high purity of the product. The diffraction peaks along with their relative intensities were found to be in good agreement with those from JCPDS (Joint Committee on Powder Diffraction Standards) card no. 10-0454 .The XRD pattern also shows broadening of peaks which is the sign of nanophase formation. The peaks (111), (220), (311) observed Bragg's angle for undoped and Mn doped CdS nanoparticles are shown in **Table 2**. It shows small shift in the peak position attributed to the local vacancies in the crystal structure [18]. According to Vegard's law, the dopant alone cannot generate an individual peak by the side of host peak but it can produce adequate shift in the position of host peak. It was understood that the host has accommodated Mn^{2+} ions into its lattice, since Mn^{2+} possesses smaller ion radii (0.66 Å) than Cd^{2+} (0.97 Å) [19]. The further small shifts in the peaks position in Mn doped CdS nanoparticles ascertain to the incorporation of Mn^{2+} into the CdS lattice and also exhibits zero alteration in the phase property of CdS. Further the electronegativities of both cations differ with sulfur, (1.55 for Mn, 1.69 for Cd, Pauling Scale) there by suggesting that Mn gets incorporated into the CdS lattice at vacancies sites most probably [20].

The calculated lattice parameter value for undoped CdS comes out to be 5.870 Å whereas for Mn doped CdS shows slightly decrease in lattice parameter with increase of Mn concentration. The average crystallite size determined using full width at half maximum (FWHM) of the diffraction peaks using Debye Scherrer's equation (1) [21] and Hall Williamson (HW) plot [21] as shown in **Fig. 3** and **Table 2**.

$$t = K\lambda / \beta_{2\theta} \cos\theta \tag{1}$$

where, t is the crystallite size, K is the Scherrer constant whose value is chosen to be unity by assuming the particle to be spherical, λ is the wavelength of X-ray beam, θ is the Bragg angle. $\beta_{2\theta}$ is the width at half the maximum intensity measured in radians.
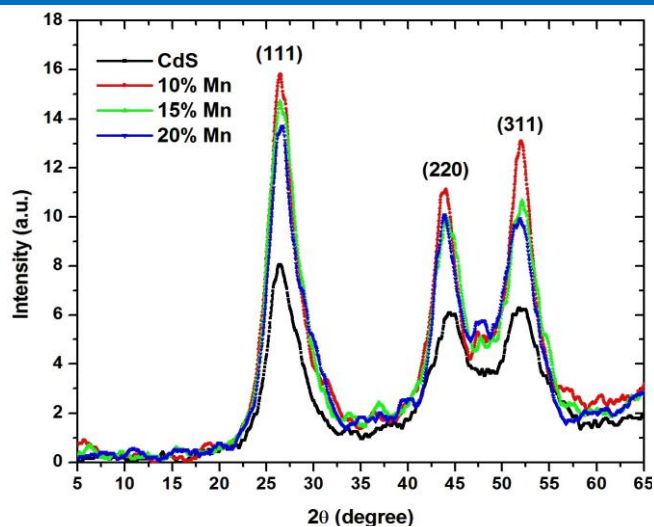

Fig. 2. XRD spectra of undoped and Mn doped CdS nanocrystallite.

Table 2. Structural parameters of undoped and Mn doped CdS samples.

Sample	2θ (degree)			a (Å)	Crystallite size(nm) Crystallite size (nm)		Strain
	(111)	(220)	(311)		Debye Scherrer's equation	HW plot	
CdS	26.425	43.625	51.100	5.870	4.43	5.08 ± 1.52	4×10⁻³
10% Mn doped CdS	26.525	43.778	52.133	5.820	3.33	2.99 ± 0.98	-0.36×10⁻³
15% Mn doped CdS	26.700	43.617	52.483	5.818	4.91	4.87 ± 1.34	-0.83×10⁻³
20% Mn doped CdS	27.067	44.550	51.900	5.806	6.05	5.30 ± 0.62	-3×10⁻³

The crystallite size was found to increase with increase in Mn concentration (**Table 2**). The estimated crystallite size was in the range between 4-6 nm. The positive sign of the strain determined from the slope of **Fig. 3** (**a**) shows that undoped CdS nanocrystallite possess tensile strain whereas negative sign of the strain for Mn doped CdS nanocrystallite indicate compressive strain for all samples.
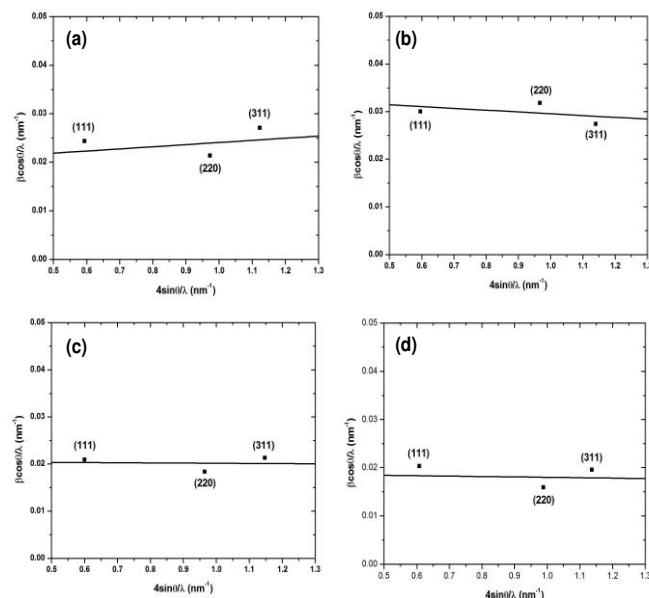

**Fig. 3.** Hall Williamson plot of undoped and Mn doped CdS samples (a) CdS (b) 10 mol % Mn doped CdS (c) 15 mol % Mn doped CdS (d) 20 mol % Mn doped CdS.

Transmission electron microscopy (TEM)

The size of as prepared undoped and Mn doped CdS nanoparticles are estimated from transmission electron microscope images as shown in **Fig. 4. (a, b, c** and **d)** respectively. The TEM images of undoped and Mn doped CdS nanoparticles appeared spherical in shape with agglomeration and having size ranging from 2 to 6 nm. No alteration in the size and shape is observed due to the incorporation of dopant but it causes the agglomeration of the particles and is found to increase with respect to dopant concentration, these results satisfactorily agree with **[22]**.
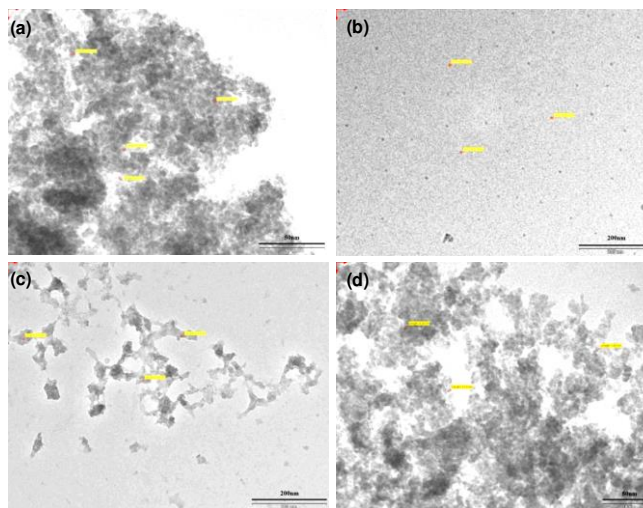
Fig. 4. TEM images of undoped and Mn doped CdS nanoparticles.(**a**) CdS (**b**) 10 mol % Mn doped CdS (**c**) 15 mol % Mn doped CdS (**d**) 20 mol % Mn doped CdS.

The agglomeration of the particles is caused by the following factors namely; reaction rate, impurities, pH, charges on the particles and solubility product constants. Separation of particles depends not only on the particle charge but also on the concentration of ions in the double layer **[23]**.

When the concentration of such ions (Cd^{2+} and Mn^{2+}) exceeds the critical value, the charge repulsion between the particles are disabled, which leads to the coagulation of double layer and results with particle agglomeration.

Fig. 5 (a, b, c, d) shows selected area electron diffraction (SAED) pattern which is indicating that undoped and Mn doped CdS nanoparticles are polycrystalline in nature. The diffracting planes are indexed as (1 1 1), (2 2 0) and (3 1 1) reflections which are corresponding to the cubic phase of CdS.

Values of interplanar spacing (d) corresponding to all diffraction rings have been calculated from the following equations

$$d = \lambda L/R \qquad (2)$$

where, R is the distance from the central bright spot to corresponding rings, L is the camera length between specimen and photographic film and λ is the wavelength of the electron based on the accelerating voltage: 200 kV = 0.02736 Å.

The lattice parameters for cubic undoped and Mn doped CdS nanoparticles are calculated from the equation:

$$a = d\ (h^2 + k^2 + l^2)^{1/2} \qquad (3)$$

where a is the lattice parameters and h, k and l are the Miller indices and d is the interplanar spacing for the plane (h k l). The lattice parameter calculated from TEM comes out to be 5.868 Å, 5.851 Å, 5.846 Å, 5.825 Å for undoped and 10, 15, 20 mol% Mn doped CdS nanoparticles respectively which closely matches with the results of XRD.
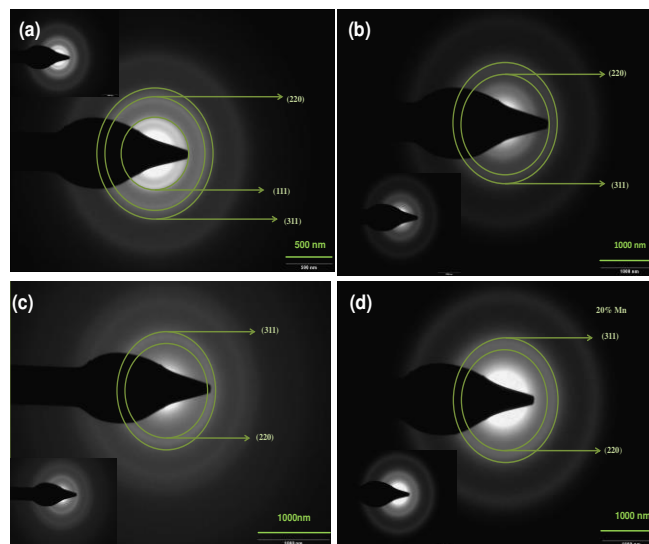

Fig. 5. Diffraction pattern of undoped and Mn doped CdS nanoparticles. (**a**) CdS (**b**) 10 mol % Mn doped CdS (**c**) 15 mol % Mn doped CdS and (**d**) 20 mol % Mn doped CdS.

Raman measurements

Raman spectra of undoped and Mn doped CdS nanoparticles recorded at room temperature are shown in **Fig. 6**. The Raman peaks of undoped CdS observed at 299.06 cm^{-1} and 596.98 cm^{-1} corresponds to the first longitudinal optical (1LO) and second longitudinal optical (2LO) phonon modes of CdS and these Raman peaks are in agreement with the reported values **[24]**.
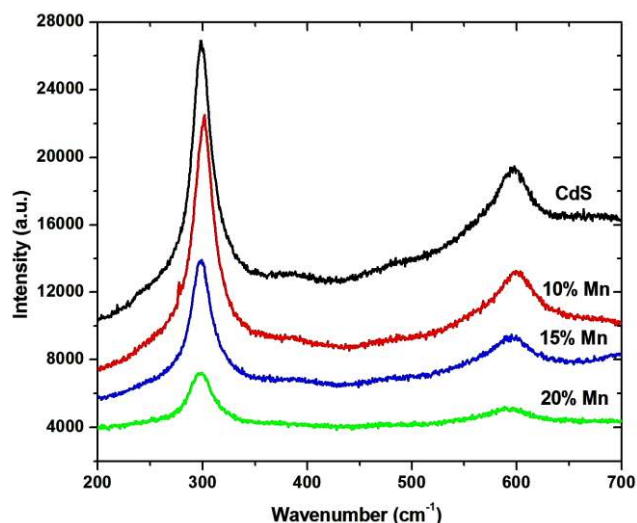

Fig. 6. Raman spectra of undoped and Mn doped CdS nanoparticles.

The Raman spectra of Mn doped CdS nanoparticles show a slight red shift when concentration of Mn increases due to the small ionic radius of Mn^{2+} ion when compared to that of Cd^{2+} ion (Mn^{2+} = 0.66 Å, Cd^{2+} = 0.97 Å) [19]. The Raman peak of 1LO and 2LO for Mn doped CdS are shown in **Table 3**.

The intensity ratio of 2LO to 1LO modes (I_{2LO}/I_{1LO}) gives the exciton–phonon coupling strength of the semiconducting materials. This intensity ratio slightly decreases as Mn^{2+} concentration increases as shown in **Fig. 6**.

Table 3. Peak position of undoped and Mn doped CdS nanoparticles.

Sample	Raman peak	
	1LO (cm^{-1})	2LO (cm^{-1})
CdS	299.06	596.98
10% Mn doped CdS	300.81	599.41
15% Mn doped CdS	298.40	595.15
20% Mn doped CdS	297.86	591.53

Table 4. Magnetic susceptibility of undoped and Mn doped CdS nanoparticles.

Sample	c_g(emu/g)	c_M(emu/mol)	η_{eff}
CdS	-0.34×10^{-6}	-48.44×10^{-4}	-
10% Mn doped CdS	4.18×10^{-6}	6.04×10^{-4}	1.21
15% Mn doped CdS	4.58×10^{-6}	6.62×10^{-4}	1.27
20% Mn doped CdS	5.48×10^{-6}	7.92×10^{-4}	1.38

Magnetic properties

Magnetic susceptibility: Magnetic Susceptibility of as prepared undoped and Mn doped CdS nanoparticles are calculated using Gouy balance. [25-29]

Gram Susceptibility of the sample was calculated using equation (4)

$$(\chi_g \times m) - (0.029 \times 10^{-6}) \times V = \tau \times (\Delta - \delta) \quad (4)$$

The volume susceptibility of air is taken as 0.029×10^{-6} per mL.

where, V = $(W_5 - W_1)/d$, $\delta = W_2 - W_1$, $\Delta = W_4 - W_3$, m = $W_3 - W_1$

(τ is the calibration standard of the tube, d is the density of water in g mL^{-1} at T, W_1 weight of empty tube, field off in g, W_2 weight of empty tube, field on in g, W_3 weight of tube filled, field off in g, W_4 weight of tube filled, field on in g, W_5 weight of tube filled with water in g.) Now, molar susceptibility is calculated by using equation

$$\chi_M = \chi_g \times M \quad (5)$$

M = Molecular weight

Effective magnetic moment is given as;

$$\eta_{eff} = 2.84(\chi_M T)^{1/2} \quad (6)$$

T = 300K

The value of χ_g, χ_M and η_{eff} calculated using above equation are shown in **Table 4**. The negative sign of χ_g for undoped CdS indicate diamagnetic behavior and positive sign of χ_g for Mn doped CdS shows paramagnetic behavior. The susceptibility varies non-linearly with concentration of Mn in CdS. At low concentration of Mn, the sp electron with opposite spin interacts with spin of CdS lattice and causes a decrease in susceptibility. At high concentrations of Mn, the d-d exchange interaction between Mn atoms dominates over the sp-d exchange interaction resulting in an abrupt increase in susceptibility [30] shown in **Fig. 7**. The effective magnetic moment increases with dopant concentration as shown in **Table 4**.
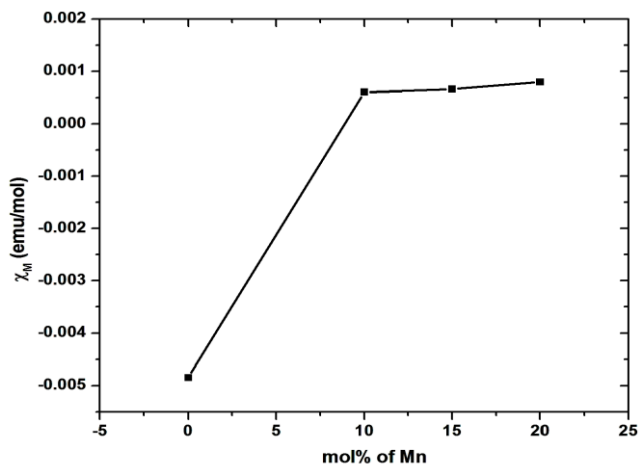

Fig. 7. Magnetic susceptibility of undoped and Mn doped CdS nanoparticles.

Vibrating sample magnetometer (VSM)

Fig. 8 shows the temperature dependence of magnetization (M-T) for only 20% Mn doped CdS sample under two different applied constant magnetic fields of 10,000 Oe and 500 Oe in the temperature range 5 K -300 K. We carried out the measurement of M-T for 20 mol% Mn doped CdS during cooling (300 K-5 K) when field was applied and removed. We also repeated the measurement from (5 K-300 K). We could observe no separation in both the cases of measurement thereby removing the probability of superparamagnetism in this material. The lowering of temperature enhances the magnetization and there is a rapid increase in magnetization taking place at temperatures below 50 K. This is assigned to paramagnetic distributions from unpaired electrons and/or isolated color centers, i.e., Mn ions isolated in the CdS crystal field and/or extrinsic defects induced by the doping.

Field dependent magnetization curve (M-H) for 20 mol% Mn doped CdS sample at 300 K and 5 K are shown in **Fig. 9**. In II-VI semiconductor nanomaterials, the nature of the magnetic properties depends on the magnitude of the transition metal ion exchange coupling with the electronic levels. There was no hysteresis noted in these plots thereby showing that 20 % Mn-doped CdS sample exhibits paramagnetic behavior only.
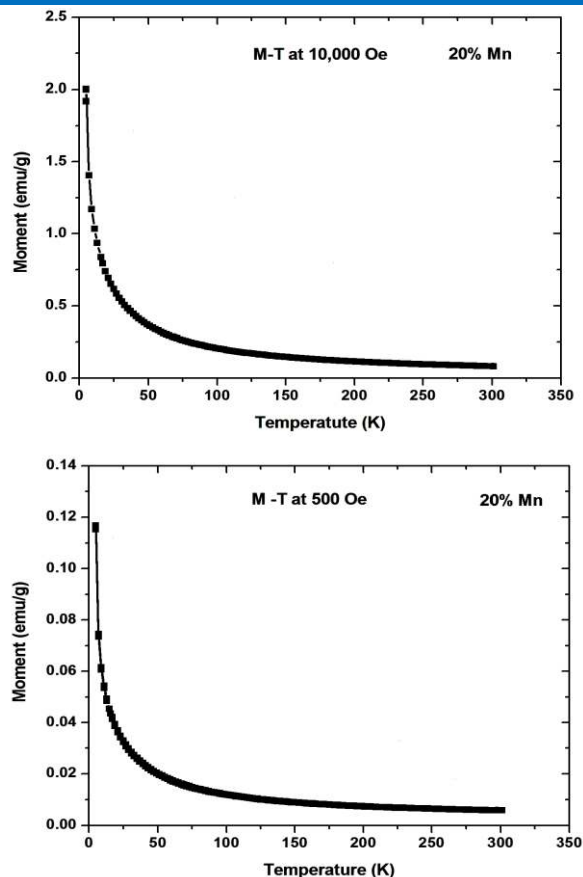
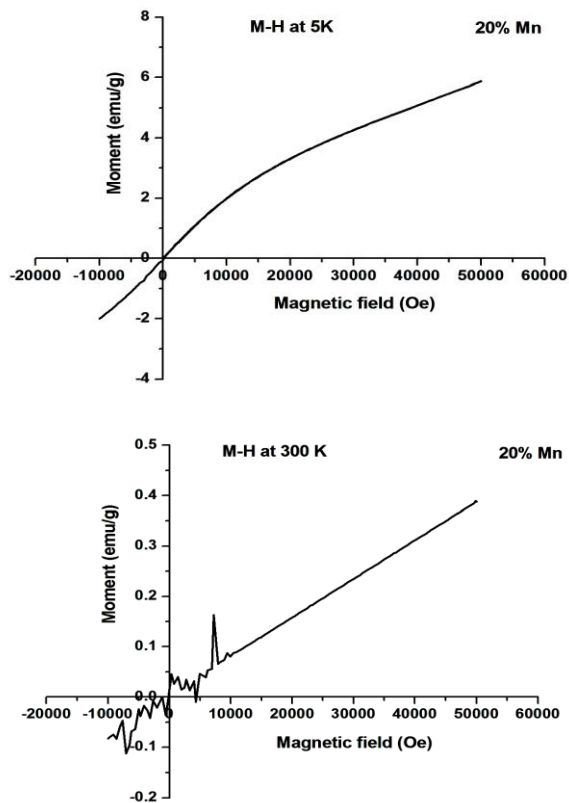**Fig. 8.** Vibrating sample magnetometer analysis M-T curves of 20 mol % Mn doped CdS sample.

Fig. 9. Vibrating sample magnetometer analysis M-H curves of 20 mol % Mn doped CdS sample.

The nature of magnetism in Mn doped CdS can be understood as follows. In this sample each Mn^{2+} has a total spin S= 5/2, originating from the half filled '3d' shells. Mn^{2+} spins are coupled by short-range anti-ferromagnetic interaction [30]. This interaction yields a series of steps at higher magnetic fields in the magnetization curves of Mn doped CdS nanoparticles. The phenomenon results in a progressive alignment of the nearest-nearest Mn pair spin components along the direction of magnetic field [1].

Conclusion

We presented here the study on structural and magnetic properties of CdS nanoparticles doped with varying Mn concentration prepared by chemical precipitation technique. The compositional analysis result showed that Cd, S and Mn are present in the samples. Structural analysis based on X-ray diffraction revealed that the undoped and Mn doped CdS samples possess cubic phase and Mn doping did not lead to the formation of manganese related secondary phase. Crystallite sizes were determined using Debye Scherrer's equation lying in the range of 4-6 nm. The SAED images showed that undoped and Mn doped CdS nanoparticles were polycrystalline in nature and size lying in the range of 2-6 nm. The longidunal optical peaks of Raman spectra of CdS nanoparticles showed red shift on Mn doping. Magnetic Susceptibility calculated by Gouy balance method showed undoped CdS nanoparticles as diamagnetic and Mn doped CdS nanoparticles to be paramagnetic in nature. M-T curves at 10,000 Oe and 500 Oe constant magnetic fields showed rapid increase in magnetization below 50 K temperature. The M-H curve at 5 K and 300 K for 20 mol % Mn doped CdS nanoparticles showed paramagnetic behavior. Hence looking at the above results doped CdS semiconductor can be extensively investigated to obtain basic information on impurity states in quantum dots and to examine their potential applications in novel light-emitting devices. CdS nanoparticles based DMS are very promising for applications in solar cells, biological labeling, spintronic devices. These nanostructures can provide innovative strategies for designing next generation energy conversion devices.

Reference

1. Venkatesu P.; Ravichandran K.; *Adv. Mat. Lett.* **2013**, *4*, 202.
   DOI: 10.5185/amlett.2012.7379
2. Wolf S. A.; Awschalom D. D.; Buhrman R. A.; Daughton J. M.; Molnár S. von; Roukes M. L.; Chtchelkanova A. Y.; Treger D. M. *Science* **2001** , *294*, 1488.
   DOI: 10.1126/science.1065389
3. Ohno H. *Science* **1998**, *281*, 951.
   DOI: 10.1126/science.281.5379.951
4. Dietl T.; Ohno H.; Matsukura F.; Cibert J.; Ferrand D. *Science* **2000**, *287*, 1019.
   DOI: 10.1126/science.287.5455.1019

5. Phuruangrat A.; Thongtem T.; Thongtem S. *Matter. Lett.* **2009**, *63*, 1538.
   DOI: 10.1016/j.matlet.2009.04.005

6. Geng J.; Jia. X.; Zhu J. *Cryst. Eng. Commun.* **2011**, *13*, 193.
   DOI: 10.1039/C0CE00180E

7. Muruganandam S., Anbalagan G., Murugadoss G., *Appl. Nanosci.* Accepted: 23 April **2014**
   DOI: 10.1007/s13204-014-0313-6

8. Kostić R.; Petrović Damjanović M.; Romčević N.; Romčević M.; Stojanović D.; Čomor M. *J. Alloys Compd.* **2012**, *521*, 134.
   DOI: 10.1016/j.jallcom.2012.01.079

9. Murase N.; Jagannathan R..; Kanematsu Y.; Watanabe M.; Kurita A.; Hirata K.; Yazawa T.; Kushida T. *J. Phys. Chem. B* **1999**, *103*, 754.
   DOI: 10.1021/jp9828179

10. Elango M.; Gopalakrishnan K.; Vairam S.; Thamilselvan M. *J. Alloys Compd.* **2012,** *538*, 48.
    DOI: 10.1016/j.jallcom.2012.05.127

11. Tripathi B.; Singh F.; Avasthi D.K.; Bhati A.K.; Das D.; Vijay Y.K. *J. Alloys Compd.* **2008**, *454*, 97.
    DOI: 10.1016/j.jallcom.2007.01.016

12. Osipyonok N.M.; Singaevsky A.F.; Noskov Yu.V.; Piryatinski Yu.P.; Smertenko P.S.; Dimitriev O.P.; Pud. A. A. *Mater. Sci. Eng. B* **2008**, *147*, 254.
    DOI: 10.1016/j.mseb.2007.08.020

13. Kulkarni J.S.; Kazakova O.;Holmes J.D. *Appl. Phys. A* **2006**, *85*, 277.
    DOI: 10.1007/s00339-006-3722-x

14. Gupta A. K.; Kripal R. *Spectrochim. Acta Part A: Molecular and Biomolecular Spectroscopy.* **2012,** *96*, 626.
    DOI: 10.1016/j.saa.2012.07.038

15. Hullavarad N.V.; Hullavarad S.S.; Karulkar P.C. *J. Nanosci. Nanotechnol.* **2008**, *8*, 3272.
    DOI: 10.1166/jnn.2008.145

16. Bhattacharyya S.; Estrin Y.; Rich D. H.; Zitoun D.; Koltypin Y.; Gedanken A. *J. Phys Chem. C* **2010**, *114*, 22002.
    DOI: 10.1021/jp107083f

17. Mishra S. K.; Srivastava R. K.; Prakash S.G.; Yadav R.S.; Panday A.C. *J. Alloys Compd.* **2012**, *513*, 118.
    DOI: 10.1016/j.jallcom.2011.10.003

18. Elango M.; Gopalakrishnan K.; Vairam S.; Thamilselvan M. *J. Alloys Compd*. **2012**, *538*, 48.
    DOI: 10.1016/j.jallcom.2012.05.127

19. Mall M.; Kumar L. *J. Lumin.* **2010**, *130*, 660.
    DOI: 10.1016/j.jlumin.2009.11.012

20. Liu M.; Du Y.; Ma L.; Jing D.; Guo L. *J. Hydrogen energy* **2011**, *3*, 730.
    DOI: 10.1016/j.ijhydene.2011.04.111

21. Deshpande M. P.; Chaki S. H.; Patel N. H.; Bhatt S. V.; Soni B. H. *J. Nano- Electron. Phys.* **2011**, *3*, 193.
    http://essuir.sumdu.edu.ua/handle/123456789/9673

22. Wang C.; Wang H.M.; Fang Z.Y. *J. Alloys Compd.* **2009**, 486, 702.
    DOI: 10.1016/j.jallcom.2009.07.043

23. Shanefield D.J. *Organic Additives and Ceramic Processing, with Applications in Powder Metallurgy Ink and Paint*, Kluwer Academic Publishers, Boston, Dordrecht, London, **1996**.

24. Fernandez J.R.L.; De Souza-Parise M.; Morais P.C. *Surface Science* **2007**, *601*, 3805.
    DOI: 10.1016/j.susc.2007.04.149

25. Figgis B.N.; Lewis J. *Modern coordination chemistry: principles and methods* Lewis J.; Wilkins R.G. (Eds.); Interscience Publishers, NY, **1960**, pp. 400.
    Ark: 13960/t55d9gq7v

26. Butler I.S.; Harrod J.F. *Inorganic Chemistry*, Redwood City, Benjamin/Cummings, **1989**, pp. 428ff

27. Dunn T.M. *Some aspects of crystal field theory*, NY, **1965** pp. 58ff.

28. Figgis B. N. *Introduction to ligand fields*; Interscience Publishers, NY, **1966**.

29. Wilkinson G.; Gillard R.D.; McClevery J.A. *Comprehensive coordination chemistry,* Oxford: Pergamon Press: **1987**, Vol. 1, pp. 256ff and 271ff.

30. Spalek J.; Lewicki A.; Tarnawski Z.; Furdyna J. K.; Galazka R. R.; Obuszko Z. *Phys. Rev. B* **1986**, *33*, 3407.
    DOI: 10.1103/PhysRevB.33.3407.